Velocity-Free Fault-Tolerant Rendezvous Law Based on Dual-Layer Adaptive Algorithm

WEI WANG[iD], YI JI[iD], DEFU LIN, XINGWEI SHI, AND JIANTING ZHAO

School of Aerospace Engineering, Beijing Institute of Technology, Beijing 100081, China
Beijing Key Laboratory of UAV Autonomous Control, Beijing 100081, China

Corresponding author: Wei Wang (wangweiyh@bit.edu.cn)

ABSTRACT Considering the scenario that the obstinate and difficult-repaired sensor and actuator failure always occurs during the spacecraft rendezvous guidance phase and may cause terrible performance, this paper studies the fault-tolerant guidance method and proposes a velocity-free guidance algorithm. Above guidance law is based on a dual-layer adaptive multi-variable super-twisting-like algorithm, where two waving gains are introduced to autonomously adjust the system trajectory subject to the relative velocity. Hence, the complex parameter selection problem is overcome. Moreover, to overcome the sensor fault in relative-velocity channel, a robust observer which can drive the velocity error converge to zero in a small finite time is presented. To test the effectiveness and stability of the proposed guidance law, considering actuator faults, second-order dynamics and saturation, numerical simulations including comparisons and Monte-Carlo are carried out and the results demonstrate above properties.

INDEX TERMS Spacecraft rendezvous, velocity-free, actuator faults, super twisting algorithm, dual-layer adaptation.

I. INTRODUCTION

Spacecrafts reliable autonomous rendezvous guidance is still a hot topic and a key technology in on-orbit docking and servicing missions [1]–[6]. During the process of rendezvous, the chaser spacecraft requires the relative position and its rate between itself and the target in real time, and then generates the desired control command and sends it to the actuators, until it arrives in the target with the same velocity. Generally speaking, rendezvous guidance can be divided into three phases, such as far-range closing, close-range closing and final mating [7]. For close-range closing phase, the well-known Clohessy-Wiltshire (C-W) differential equations [8] and Tschauner-Hempel (T-H) differential equations [9] were proposed at the middle of 20th century (C-W equations in 1959 and T-H equations in 1965) and used to describe relative dynamics for circular target orbit and elliptical target orbit, respectively. On this basis, in last century, many scholars designed quite a lot of rendezvous algorithm in earlier literature [8], [10], [11].

With the development of modern control theory, novel control techniques or algorithms are applied in spacecraft

rendezvous guidance. To name a few, to counteract the terrible influence resulted from parameter uncertainties, external perturbations, control input constraints and pole constraints, Gao *et al.* [12] proposed a multi-objective H-identify control method for the circular orbital rendezvous problem of two neighboring spacecrafts. As a supplement and improvement, [13] designed a robust H-identify rendezvous algorithm with the characteristic of non-fragileness. In above two papers, by solving a convex optimization problem, the H-identify robust controller studied can be easily obtained. To enhance overall rendezvous performance, adaptive algorithms are introduced into rendezvous scheme design. Motivated by so-called model reference adaptive control (MRAC) theory, Ulrich *et al.* [14] proposed a simple adaptive control for spacecraft proximity operations. Using a hierarchical fuzzy system and a simple adaptive algorithm, Sun and Hou [15] designed a nonlinear controller to attenuated the bad performance resulted from unknown model uncertainty and complex dynamic couplings. Considering the case that the sensors cannot measure the relative velocity accurately, Wang and Ji [16] designed an integrated relative position and attitude control for spacecraft rendezvous with input-to-state (ISS) and finite-time convergence. Combining with robust control method and adaptation,

Sun *et al.* [17] proposed a novel relative position and attitude control method for spacecraft autonomous proximity. Moreover, other advanced rendezvous algorithms were designed and applied to overcome some problem in real engineering practice. For instance, the optimal methods and algorithms were applied in [18], [19] to conserve fuel as much as possible. Reference [20] investigated the nonlinear constraints problem for the autonomous rendezvous and presented a sequential quadratic (SQ) programming to solve it. Reference [21] discussed the genetic algorithm (GA) to realize the fuel optimum for safety spacecraft rendezvous. Considering the obstacle avoidance, [22] provided a sub-optimal artificial potential function sliding mode control (SMC) based guidance law for safety proximity.

Other techniques such as backstepping design [23], $\theta - D$ method [2], [24], [25], state dependent Riccati equation (SDRE) technique [26] and SMC theory contributed much on rendezvous law design. Due to its inherent strong robustness, rapid response, low computational cost and finite-time convergent property, SMC has attracted great attention and gotten widely application in various fields. In the literature, there are many papers about SMC rendezvous scheme. To cite a few, based on time-varying SMC methodology, [27] proposed an adaptive robust rendezvous law with the properties of reaching phase elimination and globally real sliding. Reference [28] provided a nonsingular terminal sliding mode rendezvous law with an extended state observer to estimate the lumped disturbance. By using a linear quadratic optimal control method to acquire the equivalent part, [29] proposed an integral SMC technique base robust guidance law for spacecraft formation flying. Although above SMC rendezvous algorithms can meet the requirements and guarantee the performance of chaser spacecraft in autonomous rendezvous phase, the properly control-gains selection for SMC algorithms is still a difficult problem to overcome. The overestimated or underestimated parameters may result in chattering phenomenon or the loss of control, respectively. Thanks to the techniques about adaptation [30]–[32], the design parameters can be autonomously chosen according to the "distance" between the system trajectory and sliding manifold. Among these adaptive SMC algorithms, a useful systematic adjustment approach called "dual-layer adaptation" technique [33], [34] for design parameters, was proposed in recent years and applied to rapidly adjust parameters without the knowledge about external perturbation.

In this paper, a dual-layer adaptive super-twisting-like (STL) algorithm for elliptical orbital reliable spacecraft rendezvous is proposed in the presence of external disturbance, actuator failure and input saturation. First, the relative kinematics model between two neighboring spacecrafts in an arbitrary elliptical orbit is built, and a finite-time convergent observer is proposed. Next, with the reconstructed relative velocity information, a dual-layer adaptive structure based STL rendezvous law is proposed to drive the relative distance vector and its rate between the chaser and the target converge into a small neighborhood around zero, further to achieve the

reliable rendezvous. The main innovations and contributes are summarized as follows:

1). Considering the actuator faults are difficult to repair during rendezvous phase, a fault-tolerant guidance algorithm which holds a dual-layer STL structure and can autonomously adjust its parameters is proposed in this paper. The proposed guidance law holds strong robustness and shows good performance when we introduce the high-order actuator dynamics.

2). Considering the case that the relative velocity cannot be measure directly by the sensor, an FTC observer is presented to accurately estimate the relative velocity.

The rest of this paper is organized as follows: the kinematics in the presence of actuator faults and some fundamental facts are described in Sect. II, together with a finite-time convergent observer. In Sect. III, a dual-layer adaptive STL rendezvous algorithm is proposed. Numerical simulation results are given and analyzed in Sect. IV. Finally, conclusions of this paper are given in Sect. V.

II. PRELIMINARIES AND PROBLEM FORMULATION

In this section we first present several notations and preliminary results which are used throughout the whole paper. Next, kinematics of target-orbital rotating coordinate system during close-range rendezvous procession is set up, similar to [8], [16]. To describe the influence of actuator failure, the actuator command is separated into two parts: nominal manipulation part and error part. Considering the sensor fault such that the relative velocity cannot be accurately measured, a finite-time convergent observer is designed to estimate the knowledge of relative velocity. Lying on these above preliminaries, the objective of close-range closing rendezvous guidance problem is formulated.

A. PRELIMINARIES

Notations: Throughout this paper, following notations will be used. For arbitrary positive-definite matrix P, let $\lambda_{\min}(P)$ and $\lambda_{\max}(P)$ denote the minimum and maximum eigenvalues of the matrix P, respectively. For any given vector $\boldsymbol{x} = col(x_1, x_2, \ldots, x_n)$, denote the sign function as $sign(\boldsymbol{x}) = col(sign(x_1), sign(x_2), \ldots, sign(x_n))$, the absolute value as $|\boldsymbol{x}| = col(|x_1|, |x_2|, \ldots, |x_n|)$, its time derivative as $\dot{\boldsymbol{x}} = col(\dot{x}_1, \dot{x}_2, \ldots, \dot{x}_n)$, the reciprocal value as $\boldsymbol{x}^{-1} = col\left(x_1^{-1}, x_2^{-1}, \ldots, x_n^{-1}\right)$ and its 2-norm as $\|\boldsymbol{x}\| = \sqrt{\boldsymbol{x}^T \boldsymbol{x}}$. Furthermore, denote operation symbol " $\circ$ " as Hadamard product symbol (also known as the Schur product symbol or the entry wise product symbol).

Lemma 1 [35]: Assume that $V(x)$ is a C^1 smooth function which is positive definite on $U \subset \mathbb{R}^n$. For any parameters $\beta_1 > 0$ and $\beta_2 \in (0, 1)$ which satisfy $\dot{V}(x) + \beta_1 V^{\beta_2}(x) \leq 0$ on $U \subset \mathbb{R}^n$, there exists a region $U_0 \subset \mathbb{R}^n$ such that any $V(x)$ starting from $U_0 \subset \mathbb{R}^n$ can converge to zero in a finite time $T_{reach} \leq V^{1-\beta_2}(x_0)/[\beta_1(1-\beta_2)]$.

Lemma 2 [36]: Assume that $V(x)$ is a C^1 smooth function which is positive definite on $U \subset \mathbb{R}^n$. For any parameters

$\beta_1 > 0$ and $\beta_2 \in (0, 1)$ defining on $U \subset \mathbb{R}^n$ and satisfying $\dot{V}(x) + \beta_3 V(x) + \beta_1 V^{\beta_2}(x) \leq 0$, there exists a region $U_0 \subset \mathbb{R}^n$ such that any $V(x)$ starting from $U_0 \subset \mathbb{R}^n$ can converge to zero in a finite time $T_{reach} \leq \ln\left(\beta_3 V^{1-\beta_2}(x_0)/\beta_1 + 1\right)/[\beta_3(1 - \beta_2)]$.

Lemma 3 [37] (Young's Inequality): For any $x, y \in R$ and $c, d > 0$, following inequality holds

$$|x|^c |y|^d \leq \frac{c}{c+d}|x|^{c+d} + \frac{c}{c+d}|y|^{c+d} \quad (1)$$

Lemma 4 (Young's Inequality): For any semi-positive definite $x, y \in R$, there exist $p, q \in R$ which satisfy $p > 1$ and $1/p + 1/q = 1$. Then, following inequality holds

$$ab \leq a^p/p + b^q/q \quad (2)$$

Lemma 5 (Rayleigh's Inequality): For any function $f(x) = x^T P x$ where n-dimensional nonsingular matrix P is positive-definite, following inequality holds

$$\lambda_{\min}(P)\,||x||^2 \leq f(x) \leq \lambda_{\max}(P)\,||x||^2 \quad (3)$$

B. KINEMATICS OF TARGET-ORBITAL ROTATING COORDINATE SYSTEM

Assume that the chaser spacecraft is equipped with a high-performance low-level attitude control system (chattering measurement instrument and chattering suppressor for example) to keep attitude stability, whilst omitting the tiny time delay between command generator and actuators. The objective of this paper is designing a reliable robust guidance law to drive the chaser to the target with the same velocity during close-range rendezvous phase, especially when actuators cannot perform as usual.
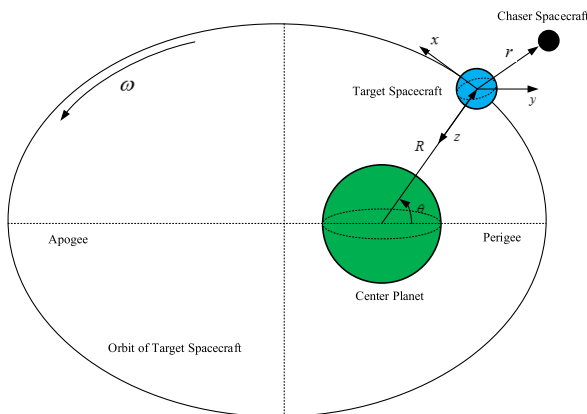
FIGURE 1. Target-orbital rotating coordinate system.

The relationship among center planet, chaser spacecraft and target spacecraft are shown as Fig.1. Regarding the center planet, the chaser and the target as point masses, thus, $r \in \mathbb{R}^3$ and $R \in \mathbb{R}^3$ denote the distance from the target spacecraft to the chaser and the distance from the center planet to the target, respectively. $\omega \in \mathbb{R}$ represents the rotating rate around the center planet on the orbit of target spacecraft, $\theta \in \mathbb{R}$ represents the rotating angle.

Similar to [8], [16], the relative position dynamics of the chaser with respect to the target is described as:

$$\frac{d^2 r}{dt^2} = -\kappa\left(\frac{R+r}{\|R+r\|^3} - \frac{R}{\|R\|^3}\right) + u + \Delta \quad (4)$$

where κ denotes gravity constant, $u \in \mathbb{R}^3$ denotes manipulated input vector and $\Delta \in \mathbb{R}^3$ denotes external lumped disturbance which is unknown but bounded, including magnetic effect, solar radiation and circumstance disturbance.

Denoting $r = col(x, y, z)$, $u = col(u_x, u_y, u_z)$ and $\Delta = col(\Delta_x, \Delta_y, \Delta_z)$, (4) can be rewritten as

$$\ddot{x} = \omega^2 x + 2\omega\dot{z} + \dot{\omega}z - \frac{\kappa x}{\|R+r\|^3} + u_x + \Delta_x$$

$$\ddot{y} = -\frac{\kappa y}{\|R+r\|^3} + u_y + \Delta_y$$

$$\ddot{z} = \omega^2 z - \omega\dot{x} - \dot{\omega}x - \kappa\left(\frac{z-R}{\|R+r\|^3} + \frac{1}{R^2}1\right) + u_z + \Delta_z \quad (5)$$

Considering the distance between the target and the chaser is much smaller than the distance between the target and the center planet (i.e. $\|r\| << \|R\|$), (5) can be simplified as

$$\ddot{x} = \omega^2 x + 2\omega\dot{z} + \dot{\omega}z - \frac{\kappa x}{R^3} + u_x + \Delta_x$$

$$\ddot{y} = -\frac{\kappa y}{R^3} + u_y + \Delta_y$$

$$\ddot{z} = \omega^2 z - 2\omega\dot{x} - \dot{\omega}x + \frac{2\kappa z}{R^3} + u_z + \Delta_z \quad (6)$$

where R and ω can be determined by following equations, similar to [8], [16].

$$\omega = \sqrt{\frac{\kappa(1 + \varphi\cos\theta)}{R}} \quad (7)$$

$$\dot{\omega} = -2\frac{\dot{R}}{R}\omega \quad (8)$$

$$\ddot{R} = R\omega^2 - \frac{\kappa}{R^2} \quad (9)$$

where φ represents the eccentricity of the elliptical target orbit.

By denoting $v = col(\dot{x}, \dot{y}, \dot{z})$, the system (6) can be rewritten as following equations.

$$\dot{r}(t) = v(t)$$

$$\dot{v}(t) = f(r, v, t) + u(r, v, t) + \Delta(t) \quad (10)$$

where $f(r, v, t)$ is given by

$$f(r, v, t) = \begin{bmatrix} \omega^2 x + 2\omega\dot{z} + \dot{\omega}z \\ -\frac{\kappa y}{R^3} \\ \omega^2 z - 2\omega\dot{x} - \dot{\omega}x \end{bmatrix}$$

This paper strives to design a reliable guidance scheme to drive the relative distance vector r and it time derivative v converge to a small region around zero in finite time, together with rapidity, accuracy, stability and robustness.

Assumption 1: During close-range rendezvous phase, the relative distance vector between the chaser and target r has a range that $r_{\min} < r < r_{\max}$, because of the chaser's and the target's length from the shells to the point masses.

C. A NOVEL FINITE-TIME CONVERGENT ROBUST OBSERVER

When the relative position and velocity measurement system of the chaser spacecraft is lack or cannot run as usual, the system states cannot be obtained in real time. Taking this situation into account, a novel robust observer is presented in this section to estimate the real relative position and its rate.

To cope with the system (1), a novel robust observer based on finite-time convergent technique is formulated as

$$
\begin{aligned}
\dot{\hat{r}}(t) &= \hat{v}(t) + a_1 \left| r(t) - \hat{r}(t) \right|^{\frac{1}{2}} sign\left(r(t) - \hat{r}(t)\right) \\
&\quad + a_2 \left| r(t) - \hat{r}(t) \right|^{\frac{3}{2}} sign\left(r(t) - \hat{r}(t)\right) \\
\dot{\hat{v}}(t) &= a_3 sign\left(r(t) - \hat{r}(t)\right) + f(r, \hat{v}, t) + u_n(r, \hat{v}, t)
\end{aligned} \quad (11)
$$

where $\hat{r} \in \mathbb{R}^3$ and $\hat{v} \in \mathbb{R}^3$ represent the estimated values of r and υ, respectively; a_1, a_2 and a_3 are positive constants

Denote estimation errors of observer (11) as $\tilde{r}(t) = r(t) - \hat{r}(t)$, $\tilde{v}(t) = v(t) - \hat{v}(t)$. For any given initial values of states $\hat{r}(t_0)$ and $\hat{v}(t_0)$, the observer system is ultimately uniformly bounded (UUB) during the rendezvous phase.

Theorem 1: For the reconstructed controlled system (10) with the robust observer (11), the estimation errors $\tilde{r}$ and $\tilde{v}$ can converge into a small compact region around zero in a finite time.

Proof: See Appendix.

III. ADAPTIVE DUAL-LAYER MULTI-VARIABLE STL GUIDANCE SCHEME

With the characteristics of strong robustness high precision and no chattering, the well-known super twisting algorithm (STA) [39], [40] is a unique continuous second-order SMC and applied in various fields. Compared with other chattering-free sliding mode control algorithms (higher-order sliding mode for example), STA requires no information about higher-order derivatives. The conventional STA, however, contains two main drawbacks in real practice: (1) the design parameters rely on the upper bound of the lumped disturbance of the system, but this upper bound is hard to estimate in the presence of the real engineering limits; (2) the convergent rate is too small when the system is far away from the equilibrium. To overcome the first drawback, the approaches in [31], [32] introduce adaptive methodology to control the gains and consequently address the dependence on the upper bound. To cope with the second drawback, [41] introduce linear terms in STA to accelerate the convergent rate.

Motived by above works, an adaptive fast STL algorithm is presented and applied in this section. For purpose of distinct demonstration, this section is divided into two parts according to the order of the conception. To be specific, a framework of new adaptive fast STL rendezvous law with linear terms is proposed in Subsects. A; in Subsects. B, dual-layer adaptive methodology is introduced to realize the algorithm proposed STL.

A. GUIDANCE LAW BASED ON FAST STL

Substitute the reconstructed relative compact velocity information $\hat{v}$ into control system (10) and replace the real velocity information v, yielding

$$
\begin{aligned}
\dot{\hat{r}}(t) &= \hat{v}(t) \\
\dot{\hat{v}}(t) &= f(r, \hat{v}, t) + u_n(r, \hat{v}, t) + d(r, v, t)
\end{aligned} \quad (12)
$$

Define the multi-variable terminal sliding manifold as following form

$$
s = \hat{v} + b_1 r + b_2 |r|^{b_3} sign(r) \quad (13)
$$

According to [42], r and $\hat{v}$ will converge to zero if the sliding surface s converges to zero. Hence, the purpose of the guidance algorithm is transformed as forcing $s \to 0$ in finite time.

Take the derivative of (13) with respect to time yielding

$$
\begin{aligned}
\dot{s} &= \dot{\hat{v}} + b_1 \hat{v} + b_2 b_3 |r|^{b_3 - 1} \hat{v} \\
&= \bar{f}(r, \hat{v}, t) + u_n(r, \hat{v}, t) + d(r, v, t)
\end{aligned} \quad (14)
$$

with the reconstructed system state equation

$$
\bar{f}(\hat{r}, \hat{v}, t) = \begin{bmatrix} \omega^2 x + 2\omega\dot{\hat{z}} + \dot{\omega}\hat{z} + b_1 \dot{\hat{x}} + b_2 b_3 |x|^{b_3-1} \dot{\hat{x}} \\ -\dfrac{\eta \hat{y}}{R^3} + b_1 \dot{\hat{y}} + b_2 b_3 |y|^{b_3-1} \dot{\hat{y}} \\ \omega^2 z - 2\omega\dot{\hat{x}} - \dot{\omega}\hat{x} + b_1 \dot{\hat{z}} + b_2 b_3 |z|^{b_3-1} \dot{\hat{z}} \end{bmatrix} \quad (15)
$$

For reconstructed control system (14), a novel fast STL guidance law with adaptive is formulated by following equations

$$
u_n = -\boldsymbol{\alpha}(t) \circ \left(\frac{s}{\|s\|^{1/p}} + ks \right) + \boldsymbol{\varsigma} + \boldsymbol{\phi}(s, L) - \bar{f}(s, t)
$$

$$
\dot{\boldsymbol{\varsigma}} = -2\boldsymbol{\beta}(t) \circ \begin{pmatrix} \dfrac{p-1}{p} \cdot \dfrac{s}{\|s\|^{2/p}} \\ + k \cdot \left(\dfrac{2(p-1)^2}{p} + \dfrac{4(p-1)^2}{p^2} \right) \\ \cdot \dfrac{s}{\|s\|^{1/p}} + \dfrac{4(p-1)^2}{p^2} k^2 s \end{pmatrix} \quad (16)
$$

where $k > 0$ and $p > 2$ are design parameters, adaptive parameters $\boldsymbol{\alpha}(t) \in \mathbb{R}^3$ and $\boldsymbol{\beta}(t) \in \mathbb{R}^3$ are defined as

$$
\begin{aligned}
\boldsymbol{\alpha}(t) &= \boldsymbol{L}^n(t)\alpha_0 \\
\boldsymbol{\beta}(t) &= \boldsymbol{L}^{2n}(t)\beta_0
\end{aligned} \quad (17)
$$

where $\boldsymbol{L}(t) \in \mathbb{R}^3$ is adaptive element vector, α_0, β_0 and n are positive constants. Moreover, compensation function $\boldsymbol{\phi}(s, L)$ is given by

$$
\boldsymbol{\phi}(s, L) = -n\dot{\boldsymbol{L}}(t) \circ \boldsymbol{L}^{-1}(t) \circ \left(\frac{\left(\|s\|^{-\frac{1}{p}} + \frac{2(p-1)}{p} k_2 \right) s}{\frac{p-1}{p} \|s\|^{-\frac{1}{p}} + \frac{2(p-1)}{p} k_2} \right) \quad (18)
$$

Theorem 2: Define following matrices as

$$A_2 = \begin{bmatrix} -\frac{1}{2}\alpha_0 & \frac{1}{2} \\ -\beta_0 & 0 \end{bmatrix}, \quad B_2 = \begin{bmatrix} 0 \\ 1 \end{bmatrix},$$

$$C_2 = [1 \quad 0], \quad P_2 = \begin{bmatrix} p_{11} & p_{12} \\ p_{21} & p_{22} \end{bmatrix} \tag{19}$$

where P_2 is a symmetric positive definite matrix (i.e. $p_{12} = p_{21}$) and satisfies $p_{11} > 0$, $p_{22} > 0$ and $p_{12}p_{21} < p_{11}p_{22}$.

Take system (10), sliding manifold (13) and manipulated variable (16) into consideration, assume that adaptive element vector $L(t)$ is bounded and selected so as to enforce that $L^{2n}(t) > \max\{L_0, \dot{d}\}$, where L_0 denotes as a positive constant, then a real second-order sliding mode will occur to drive the sliding manifold (13) converge to zero in a finite time if the gains α_0 and β_0 are selected so that $P_2A_2 + A_2^T P_2 + \mu P_2 + P_2 B_2 B_2^T P_2 + C_2^T C_2 < 0$.

Proof: Note that the proposed rendezvous scheme is a nonlinear compound observer-controller system and cannot satisfy the well-known separation principle. Thanks to the works in [43], a properly chosen finite-time-bounded (FTB) Lyapunov function candidate is enough to overcome this problem. With above fact in mind, the proof should be divided into three steps. The UUB property is demonstrated via a FTB Lyapunov function candidate in step I; the finite-time reaching property (the system trajectory reaching to the sliding manifold in a finite time) is demonstrated by Lyapunov method in step II; the finite-time reaching property (the relative position and its rate converging into some vicinity around zero) is demonstrated by Lyapunov method in step III.

Step I: Substituting (A.1) into system (14) yields

$$\dot{s} = -\alpha(t) \circ \left(\frac{s}{\|s\|^{1/p}} + \frac{2(p-1)}{p}ks \right) + \phi(s, L)$$

$$+ \int_0^v \xi(r, v, t)dv$$

$$- \int_0^v 2\beta(t) \circ \begin{pmatrix} \frac{p-1}{p} \cdot \frac{s}{\|s\|^{2/p}} + k \\ \cdot \left(\frac{2(p-1)^2}{p} + \frac{4(p-1)^2}{p^2} \right) \\ \cdot \frac{s}{\|s\|^{1/p}} + \frac{4(p-1)^2}{p^2}k^2 s \end{pmatrix} dv \tag{20}$$

with the term $\int_0^v \xi(r, v, t)dv = d(r, v, t)$. For ease of system stability analysis, select an auxiliary vector as follows:

$$\eta = col(\eta_1, \eta_2) = col\left(L^n \circ \left(\frac{s}{\|s\|^{1/p}} + \frac{2(p-1)}{p}ks \right), \varsigma + d \right) \tag{21}$$

Thus, (14) can be formulated as following equation through the auxiliary vector.

$$\dot{s} = -\alpha_0 \eta_1 + \eta_2 + \phi(s, L) \tag{22}$$

Taking the derivative of (22) with respect to time yields

$$\dot{\eta}_1 = nL^{n-1} \circ \dot{L} \circ \left(\frac{s}{\|s\|^{1/p}} + \frac{2(p-1)}{p}ks \right)$$

$$+ L^n \circ \left(\frac{p-1}{p} \frac{1}{\|s\|^{1/p}} + \frac{2(p-1)}{p}k \right)$$

$$\times \left(-\alpha(t) \left(\frac{s}{\|s\|^{1/p}} + \frac{2(p-1)}{p}ks \right) + \eta_2 + \phi \right)$$

$$\dot{\eta}_2 = -2\beta(t) \circ \begin{pmatrix} \frac{p-1}{p} \cdot \frac{s}{\|s\|^{2/p}} + k \\ \cdot \left(\frac{2(p-1)^2}{p} + \frac{4(p-1)^2}{p^2} \right) \\ \cdot \frac{s}{\|s\|^{1/p}} + \frac{4(p-1)^2}{p^2}k^2 s \end{pmatrix}$$

$$+ \xi(r, v, t) \tag{23}$$

It follows from (21) that there holds following equation

$$nL^{n-1} \circ \dot{L} \circ \left(\frac{s}{\|s\|^{1/p}} + \frac{2(p-1)}{p}ks \right)$$

$$+ L^n \circ \left(\frac{p-1}{p} \frac{1}{\|s\|^{1/p}} + \frac{2(p-1)}{p}k \right) \phi = 0 \tag{24}$$

(24) can be rewritten as following form

$$\dot{\eta}_1 = \left(\frac{p-1}{p} \frac{1}{\|s\|^{1/p}} + \frac{2(p-1)}{p}k \right)(-\alpha(t)\eta_1 + L^n \circ \eta_2)$$

$$\dot{\eta}_2 = -\left(\frac{2(p-1)}{p} \frac{1}{\|s\|^{1/p}} + \frac{4(p-1)}{p}k \right)\beta(t) L^n \circ \eta_1$$

$$+ \xi(r, v, t) \tag{25}$$

Further, it can be rewritten as

$$\dot{\eta}_1 = L^n \circ \left(\frac{p-1}{p} \frac{1}{\|s\|^{1/p}} + \frac{2(p-1)}{p}k_2 \right)$$

$$\times \left(-\frac{1}{2}\alpha(t) \circ L^{-n} \circ \eta_1 + \frac{1}{2}\eta_2 \right)$$

$$\dot{\eta}_2 = L^n \circ \left(\frac{p-1}{p} \frac{1}{\|s\|^{1/p}} + \frac{2(p-1)}{p}k_2 \right)$$

$$\times \left(-\beta(t) \circ L^{-2n} \circ \eta_1 + \bar{\xi}(r, v, t) \right) \tag{26}$$

with

$$\bar{\xi}(r, v, t) = \frac{\xi(r, v, t) \circ L^{-n}(t)}{\left(\frac{p-1}{p} \frac{1}{\|s\|^{1/p}} + \frac{2(p-1)}{p}k_2 \right)} \tag{27}$$

Take a Lyapunov function candidate $V_2 = \frac{1}{2}\|\eta\|^2 + \frac{1}{2}\|e\|^2$ into account and its time derivative can be formulated as

$$\dot{V}_2 = \eta_1^T \dot{\eta}_1 + \eta_2^T \dot{\eta}_2 + \frac{1}{2}\dot{V}_1$$

$$= K \circ \left(\begin{array}{l} \left(-\frac{1}{2}\alpha(t) \circ L^{-n} \circ \eta_1 + \frac{1}{2}\eta_2 \right) \circ \eta_1 \\ + \left(-\beta(t) \circ L^{-2n} \circ \eta_1 + \bar{\xi}(r, v, t) \right) \circ \eta_2 \end{array} \right)$$

$$+ \frac{1}{2}\dot{V}_1$$

$$\leq K \circ \left(-\frac{1}{2}\alpha_0\eta_1^2 + \left(\frac{1}{2} - \beta_0 \right)\eta_1 \circ \eta_2 + \bar{\xi}(r, v, t) \circ \eta_2 \right)$$

$$+ \frac{1}{2}\dot{V}_1 \tag{28}$$

with $K(s) = L^n \left(\frac{p-1}{p} \frac{1}{\|s\|^{1/p}} + \frac{2(p-1)}{p} k \right)$. Since that $L(t)$ is a UUB function and $\|s\|$ has its minimum value according to Assumption 1, the maximum value of K can be formulated as $K_{\max} = L^n \left(\frac{p-1}{p} \frac{1}{\|s\|_{\min}^{1/p}} + \frac{2(p-1)}{p} k \right)$.

Hence, (28) is rewritten as

$$\dot{V}_2 \leq K_{\max} \circ \left(-\frac{1}{2} \alpha_0 \eta_1^2 + \left(\frac{1}{2} - \beta_0 \right) \eta_1 \circ \eta_2 + \bar{\xi}(r, v, t) \circ \eta_2 \right)$$
$$+ \frac{1}{2} \dot{V}_1$$
$$\leq K_{\max} \left(\frac{1}{2} \alpha_0 \| \eta_1 \|^2 + \left| \frac{1}{2} - \beta_0 \right| \| \eta_1 \| \| \eta_2 \| \right.$$
$$\left. + \| \bar{\xi}(r, v, t) \| \| \eta_2 \| \right) + \frac{1}{2} \dot{V}_1$$
$$\leq K_{\max} \left(\frac{1}{2} \alpha_0 \| \eta_1 \|^2 + \left| \frac{1}{2} - \beta_0 \right| \| \eta_1 \| \| \eta_2 \| \right.$$
$$\left. + \| \bar{\xi}(r, v, t) \| \| \eta_2 \| \right) - \frac{\Omega}{\lambda_{\max}(P)} V_1^{\frac{1}{2}}$$
$$\leq K_{\max} \left(\frac{1}{2} \alpha_0 \| \eta_1 \|^2 + \left| \frac{1}{2} - \beta_0 \right| \| \eta_1 \| \| \eta_2 \| \right.$$
$$\left. + \| \bar{\xi}(r, v, t) \| \| \eta_2 \| \right) \qquad (29)$$

Then, in the case of $\| \eta_2 \| \geq \| \bar{\xi}(r, v, t) \|$, inequality (29) can be rewritten as

$$\dot{V}_2 \leq K_{\max} \left(\frac{1}{2} \alpha_0 \| \eta_1 \|^2 + \left| \frac{1}{2} - \beta_0 \right| \| \eta_1 \| \| \eta_2 \| + \| \eta_2 \|^2 \right)$$
$$\leq K_{\max} \left(\frac{1}{2} \alpha_0 \| \eta_1 \|^2 + \left| \frac{1}{4} - \frac{\beta_0}{2} \right| \| \eta_1 \|^2 \right.$$
$$\left. + \left| \frac{1}{4} - \frac{\beta_0}{2} \right| \| \eta_2 \|^2 + \| \eta_2 \|^2 \right)$$
$$\leq K_{\max} \varpi_1 \left(\frac{1}{2} \| \eta \|^2 \right) + \varpi_1 K_{\max} \circ V_1$$
$$= \varpi_1 K_{\max} \circ V_2 \qquad (30)$$

with $\varpi_1 = \max \{ \alpha_0 + |0.5 - \beta_0|, 2 + |0.5 - \beta_0| \}$ is a certain constant.

In the case of $\| \eta_2 \| < \| \bar{\xi}(r, v, t) \|$, inequality (30) can be rewritten as

$$\dot{V}_2 \leq K_{\max} \left(\frac{1}{2} \alpha_0 \| \eta_1 \|^2 + \left| \frac{1}{2} - \beta_0 \right| \| \eta_1 \| \| \bar{\xi}(r, v, t) \| \right.$$
$$\left. + \| \bar{\xi}(r, v, t) \|^2 \right)$$
$$\leq K_{\max} \left(\frac{1}{2} \alpha_0 \| \eta_1 \|^2 + \left| \frac{1}{4} - \frac{\beta_0}{2} \right| \| \eta_1 \|^2 \right.$$
$$\left. + \left| \frac{1}{4} - \frac{\beta_0}{2} \right| \| \bar{\xi}(r, v, t) \|^2 + \| \bar{\xi}(r, v, t) \|^2 \right)$$
$$= K_{\max} \left(\left(\frac{1}{2} \alpha_0 + \left| \frac{1}{4} - \frac{\beta_0}{2} \right| \right) \| \eta_1 \|^2 \right)$$
$$+ K_{\max} \left(1 + \left| \frac{1}{4} - \frac{\beta_0}{2} \right| \right) \| \bar{\xi}(r, v, t) \|^2$$

$$\leq K_{\max} \varpi_2 \left(\frac{1}{2} \| \eta_1 \|^2 + \frac{1}{2} \| \eta_1 \|_1^2 \right) + \frac{1}{2} V \circ K_{\max}$$
$$+ K_{\max} \left(1 + \left| \frac{1}{4} - \frac{\beta_0}{2} \right| \right) \| \bar{\xi}(r, v, t) \|_{\max}^2$$
$$\leq \varpi_2 K_{\max} \circ V_2 + M_{\max} \qquad (31)$$

with $\varpi_2 = \alpha_0 + |0.5 - \beta_0|$ and $M_{\max} = K_{\max} \left(1 + \left| \frac{1}{4} - \frac{\beta_0}{2} \right| \right) \| \bar{\xi}(r, v, t) \|_{\max}^2$. Combining with (12) and (31) yields

$$\dot{V}_2 \leq \varpi_{\max} K_{\max} \circ V_2 + M_{\max} \qquad (32)$$

where $\varpi_{\max} = \max \{ \varpi_1, \varpi_2 \}$. Solving (32) in an arbitrary time domain $[0, t]$ gives

$$V_2(t) \leq \left[V_2(0) + \frac{K_{\max}^{-1} \circ M_{\max}}{\varpi_{\max}} \right] e^{K_{\max} \varpi_{\max} t}$$
$$- \frac{K_{\max}^{-1} \circ M_{\max}}{\varpi_{\max}} \qquad (33)$$

where $V_2(0)$ is the initial value of $V_2(t)$ at the beginning of manipulation.

(33) demonstrates the closed-system is UUB in an arbitrary time domain $[0, t]$.

Step II: Note that (11) can be rewritten as following matrix form

$$\dot{\eta} = K_{\max}(A_0 \eta + B_0 \bar{\xi}) \qquad (34)$$

where, $K_{\max}$ is the maximum of all the elements in $K_{\max}$, i.e. $K_{\max} = \max \{ K_{1\max}, K_{2\max}, K_{3\max} \}$. Select a Lyapunov function candidate as $V_3 = \eta^T P_0 \eta$, take its time derivative yields

$$\dot{V}_3 = K_{\max}(\eta^T (A_0^T P_0 + P_0 A_0) \eta + 2\eta^T P_0 B_0 \bar{\xi}) \qquad (35)$$

According to Lemma 4

$$\dot{V}_3 \leq K_{\max} \left(\eta^T \left(A_0^T P_0 + P_0 A_0 + P_0 B_0 B_0^T P_0 \right) \eta + \| \bar{\xi} \|^2 \right) \qquad (36)$$

It follows from (12) that

$$\| \bar{\xi}(r, v, t) \| = \left\| \frac{p \| s \|^{1/p} \xi(r, v, t) \circ L^{-n}(t)}{(p - 1 + 2(p-1)k_2 \| s \|^{1/p})} \right\|$$
$$\leq \frac{\| \xi(r, v, t) \|}{\| L^{2n}(t) \|} \| \eta_1 \| \qquad (37)$$

Considering the fact in Lemma 5, one can conclude that $\| \bar{\xi}(t) \| \leq \frac{\| \xi(t) \|}{\| L^{2n} \|} \| \eta_1 \| \leq \| \eta_1 \|$. Hence, there exists

$$\dot{V}_3 \leq K_{\max} \left(\eta^T \left(A_0^T P_0 + P_0 A_0 + P_0 B_0 B_0^T P_0 \right) \eta + \eta_1^T \eta_1 \right)$$
$$= K_{\max} \eta^T \left(A_0^T P_0 + P_0 A_0 + P_0 B_0 B_0^T P_0 + C_0^T C_0 \right) \eta \qquad (38)$$

Assuming that the gains α_0 and β_0 is chosen so that the inequality (18) holds, yields

$$\dot{V}_3 \leq -\frac{p-1}{p} \frac{\mu \| L^n \|}{\| s \|^{1/p}} V_3^{(p-2)/(p-1)} - \frac{2(p-1)}{p} \mu k_2 \| L^n \| V_3 \qquad (39)$$

If follows the facts $\lambda_{\min}(P)\|\boldsymbol{\eta}\|^2 \le V_3 \le \lambda_{\max}(P)\|\boldsymbol{\eta}\|^2$ and $L^n\|s\|^{(p-1)/p} < \|\boldsymbol{\eta}_1\|$ (from the definition of $\boldsymbol{\eta}_1$) that $\|s\|^{1/p} \le \left(\frac{V_3}{\lambda_{\min}(P)L^n}\right)^{\frac{1}{p-1}}$, further, one can conclude that

$$
\dot{V}_3 \le -\frac{p-1}{p}\mu L^{pn/(p-1)}\left(\lambda_{\min}^{1/(p-1)}(P)\right)V_3^{(p-2)/(p-1)}
$$
$$
-\frac{2(p-1)}{p}\mu L^n k_2\, V_3
$$
$$
= -\chi_1\, V_3^{(p-2)/(p-1)} - \chi_2 V_3 \tag{40}
$$

According to Lemma 2, one can know that the system trajectory can reach to the sliding manifold s in a finite time.

Step III: At the time that the system trajectory reaches to sliding manifold (13), there holds following equation.

$$
\hat{\boldsymbol{v}} + b_1 \boldsymbol{r} + b_2 |\boldsymbol{r}|^{b_3} \, sign(\boldsymbol{r}) = 0 \tag{41}
$$

For system (21), chose a Lyapunov function candidate as

$$
V_4 = \frac{1}{2}\|\boldsymbol{r}\|^2 \tag{42}
$$

Taking the derivative of (42) with respect to time yields

$$
\dot{V}_4 = \boldsymbol{r}^T \hat{\boldsymbol{v}} = -b_1 \boldsymbol{r}^T \boldsymbol{r} - b_2 \left|\boldsymbol{r}^T\right|^{b_3}|\boldsymbol{r}|
$$
$$
\le -2b_1 V_4 - 2b_2 V_4^{\frac{b_3+1}{2}} \tag{43}
$$

According to Lemma 2, one can know that the sliding manifold can force system state $\hat{\upsilon}$ converge into a small compact region around zero in a finite time.

This completes the proof.

B. DUAL-LAYER ADAPTION FUNCTION DESIGN

From last section we know that with a properly chosen bounded adaptive function $L(t)$ satisfying $L^{2n}(t) > \max\{L_0, \|\boldsymbol{\xi}\|\}$, the proposed rendezvous scheme can drive the system state vectors $\hat{\boldsymbol{r}}$ and $\hat{\boldsymbol{v}}$ convergence in a small neighborhood around the origin. Now a question arises: how to design the adaptive function $L(t)$? Motivated by so-called dual layer adaptive algorithm [33], [34], in this section we will give a new dual layer adaptive function with a novel design method.

The so-called dual layer approaches in [33], [34] relies on so-called equivalent control technique [31].

Considering (38), by the conception of so-called equivalent control, $\dot{\boldsymbol{\eta}}_2 \equiv \boldsymbol{0}$ holds when the system trajectory reaches to the sliding manifold vector and then sliding on it. Hence, the switching function vector $[s/\|s\|]_{eq}$ is govern by

$$
\boldsymbol{u}_{eq} = 2\boldsymbol{\beta}(s)\circ[s/\|s\|]_{eq}\|s\|^{1-2/q}+2\boldsymbol{\beta}(s)\,\psi(s)\circ[s/\|s\|]_{eq}
$$
$$
= \boldsymbol{\xi}(t) \tag{44}
$$

with function $\psi(s) = \left(\frac{p-1}{p}\cdot\|s\|^{1-2/q} + k_2\cdot\frac{p+1}{p-1}\cdot\|s\|^{1-1/q}\right.$ $\left. + k_2^2\|s\|\right)$. Where $[s/\|s\|]_{eq}$ is usually referred to as the equivalent control and denotes the average value of $s/\|s\|$ which must maintain the sliding conditions. However, as

a theoretic conception which only existed in ideal circumstances, $[s/\|s\|]_{eq}$ cannot be accurately measured or calculated in real time. Thanks to low pass filtering technology, we can approximately estimate it by using following first-order differentiator with switched signal [31]

$$
\dot{\bar{\boldsymbol{\vartheta}}}_{eq} = \frac{1}{\tau}\left(\frac{s}{\|s\|} - \bar{\boldsymbol{\vartheta}}_{eq}\right) \tag{45}
$$

where τ is an arbitrary positive constant which represents the frequency of low pass filter. Moreover, $\bar{\boldsymbol{\vartheta}}_{eq}$ represents the estimated value of $[s/\|s\|]_{eq}$. As a result, we can precisely estimate the bounded total disturbance $\boldsymbol{\xi}(r,v,t)$.

Similar to [33], [34], for ease of analysis, define a new vector variable as

$$
\boldsymbol{\delta}(t) = \boldsymbol{L}(t) - \frac{1}{m\beta_0}|\boldsymbol{\vartheta}_{eq}(t)| - \boldsymbol{\varepsilon} \tag{46}
$$

where $0 < m < 1/\beta_0 < 1$ is a positive design parameter and $\boldsymbol{\varepsilon} = col(\varepsilon_0, \varepsilon_0, \varepsilon_0)$. Then, define adaptive control element $\boldsymbol{L}(t)$ as

$$
\boldsymbol{L}(t) = \boldsymbol{l}_0 + \boldsymbol{l}(t) \tag{47}
$$

where $\boldsymbol{l}_0 = col(l_0, l_0, l_0)$ is a small positive vector and $\boldsymbol{l}(t)$ is updated by

$$
\dot{\boldsymbol{l}}(t) = -\boldsymbol{\rho}(t)\, sign(\boldsymbol{\delta}) \tag{48}
$$

with

$$
\boldsymbol{\rho}(t) = \boldsymbol{n}_0 + \boldsymbol{n}(t) \tag{49}
$$

where $\boldsymbol{r}_0 = col(n_0, n_0, n_0)$ and $\boldsymbol{n}(t)$ is updated by

$$
\dot{\boldsymbol{n}}(t) = \gamma\,|\boldsymbol{\delta}(t)| \tag{50}
$$

where $\gamma > 0$ is design parameter.

Theorem 3: Take into account the system (13) subject to lumped uncertainty vector $\boldsymbol{d}(t)$ and its time derivative $\boldsymbol{\xi}(t)$ which satisfy $\|\boldsymbol{\xi}(t)\| \le m_0$ and $\|\dot{\boldsymbol{\xi}}(t)\| \le m_1$. The dual-layer adaptive algorithm in (46) $\sim$ (50) ensures that the adaptive element vector $\boldsymbol{L}(t) \ge |\boldsymbol{\xi}(t)|$ in finite time and $\boldsymbol{L}(t)$ is also UUB.

Proof: For the convenience of demonstration, an auxiliary variable is defined as

$$
\boldsymbol{\sigma}(t) = col\left(\frac{m_1}{m\beta_0},\frac{m_1}{m\beta_0},\frac{m_1}{m\beta_0}\right) - \boldsymbol{n}(t) \tag{51}
$$

Taking the derivative of $\boldsymbol{\delta}(t)$ with respect to time yields

$$
\dot{\boldsymbol{\delta}}(t) = \dot{\boldsymbol{l}}(t) - \frac{1}{m\beta_0}\frac{d}{dt}|\boldsymbol{\vartheta}_{eq}(t)|
$$
$$
= \dot{\boldsymbol{l}}(t) - \frac{1}{m\beta_0}\frac{d}{dt}|\boldsymbol{\xi}(t)| \tag{52}
$$

Further, it follows from (51) and (52) that

$$
\boldsymbol{\delta}(t)\dot{\boldsymbol{\delta}}(t) \le \boldsymbol{\delta}(t)\dot{\boldsymbol{l}}(t) + \frac{m_1}{m\beta_0}|\boldsymbol{\delta}(t)|
$$
$$
= -n_0|\boldsymbol{\delta}(t)| - \boldsymbol{n}(t)|\boldsymbol{\delta}(t)| + \frac{n_1}{n\beta_0}|\boldsymbol{\delta}(t)|
$$
$$
= -n_0|\boldsymbol{\delta}(t)| + \boldsymbol{\sigma}(t)|\boldsymbol{\delta}(t)| \tag{53}
$$

In order to discuss the ultimate uniform global boundedness of the dynamical system, following Lyapunov function candidate can be taken into account.

$$V_5 = \frac{1}{2}\|\boldsymbol{\delta}\|^2 + \frac{1}{2\gamma}\|\boldsymbol{\sigma}\|^2 \qquad (54)$$

Taking its derivative along the trajectories of $\boldsymbol{\delta}(t)$ and $\boldsymbol{\sigma}(t)$ it follows that

$$\dot{V}_5 = \boldsymbol{\delta}\dot{\boldsymbol{\delta}} + \frac{1}{\gamma}\boldsymbol{\sigma}\dot{\boldsymbol{\sigma}}$$

$$\leq -n_0\,|\boldsymbol{\delta}(t)| + \boldsymbol{\sigma}(t)\,|\boldsymbol{\delta}(t)| + \frac{1}{\gamma}\boldsymbol{\sigma}(t)\cdot(-\gamma\,|\boldsymbol{\delta}(t)|)$$

$$= -n_0\,|\boldsymbol{\delta}(t)| \qquad (55)$$

Since $\dot{V}_5 \leq 0$, one can imply that $\boldsymbol{\delta}(t)$ and $\boldsymbol{\sigma}(t)$ have their own bound, further, $\boldsymbol{L}(t)$ is UUB. According to Barbalat's invariance principle, $\boldsymbol{\delta}(t) \to 0$ as $t \to \infty$. As a result, there exists a finite time t_0 such that $|\boldsymbol{\delta}(t)| \leq \varepsilon/2$ holds for $t > t_0$. It follows from the definition of $\delta(t)$ in (46) that

$$|\boldsymbol{\delta}(t)| = \left| \boldsymbol{L}(t) - \frac{1}{m\beta_0}\left|\boldsymbol{\vartheta}_{eq}(t)\right| - \boldsymbol{\varepsilon} \right| < \varepsilon/2 \qquad (56)$$

and thus

$$\boldsymbol{L}(t) - \frac{1}{m\beta_0}\left|\boldsymbol{\vartheta}_{eq}(t)\right| - \boldsymbol{\varepsilon} < -\boldsymbol{\varepsilon}/2 \qquad (57)$$

It follows from $a\beta_0 < 1$ that

$$\boldsymbol{L}(t) > \frac{1}{m\beta_0}\left|\boldsymbol{\vartheta}_{eq}(t)\right| + \frac{\boldsymbol{\varepsilon}}{2} > \left|\boldsymbol{\vartheta}_{eq}(t)\right| + \frac{\boldsymbol{\varepsilon}}{2} > |\boldsymbol{\xi}(t)| \quad (58)$$

This proves the claim of Theorem 3.

Furthermore, according to the definition of $\boldsymbol{\delta}(t)$ in (46) it follows

$$|\boldsymbol{L}(t)| < |\boldsymbol{\delta}(t)| + \frac{1}{m\beta_0}\left|\boldsymbol{\vartheta}_{eq}(t)\right| + \boldsymbol{\varepsilon} < |\boldsymbol{\delta}(t)| + \frac{m_1}{m\beta_0} + \boldsymbol{\varepsilon}$$

$$(59)$$

So that $\boldsymbol{L}(t)$ is UUB.

This completes the proof.

Remark 1: From above proof processes, one can clearly see that there exists a dual-layer structure ((46) ~ (49)). It follows from (46) that

$$\boldsymbol{L}(t) > \left|\boldsymbol{\vartheta}_{eq}(t)\right| + \frac{1-m\beta_0}{m\beta_0}\left|\boldsymbol{\vartheta}_{eq}(t)\right| + \frac{\boldsymbol{\varepsilon}}{2} \qquad (60)$$

The term $\boldsymbol{\varepsilon}$ and the parameter a are properly chosen so as to guarantee that $\boldsymbol{L}(t)$ is larger than the upper bound of the lumped disturbance during the whole rendezvous. Also in [33], [34], the term $\frac{1-m\beta_0}{m\beta_0}\left|\boldsymbol{\vartheta}_{eq}(t)\right| + \frac{\varepsilon}{2}$ is called "safety margin".

Remark 2: From the control algorithm (16) ~ (18) and the dual-layer structure (46) ~ (49), one can imply that the proposed rendezvous scheme requires no information about the upper bound of the lumped disturbance. Due to its inherent characteristic of strong robustness, the proposed STL algorithm can resist the external disturbance with highly

efficiency, while the dual-layer structure can seek the upper bound of lumped disturbance autonomously. Considering the circumstance condition (vacuum state) in real practice scenario, the external perturbation and the actuator fault is always smaller than the safety margin. Hence, the proposed algorithm can be well used in real rendezvous, at least in theory.

IV. CASES STUDY

Based on dual-layer adaptive algorithm, an "observer-controller" system was proposed in the above considering the characteristics of the actuator, including command saturation, accumulating and abrupt fault, time-delay. To test the effectiveness and robustness of the proposed guidance algorithm for reliable rendezvous, several numerical simulation examples which imitate the close-range closing phase in an elliptical orbital spacecraft rendezvous mission are carried out. The simulations are performed by using a fourth-order Runge-Kutta solver with a fixed step size 0.005s.

The simulations are organized as follows: first, the flow chart of the proposed system, the external disturbance, the orbital and design parameters are presented in Section A; next, to test the fault-tolerant property and actuator dynamics adaptation of proposed rendezvous guidance system, simulations respectively considering actuator fault and second-order actuator dynamics are carried out in Section B and C; finally, to demonstrate the robustness of proposed rendezvous guidance law, Monte-Carlo simulations are carried out in Section D.
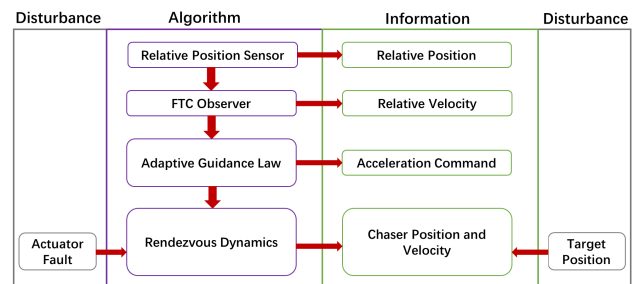
FIGURE 2. The implementation flow-chart of proposed rendezvous guidance law.

A. SIMULATION SETUP

The implementation flow-chart is shown as Figure.2: first, the sensor measures the relative position information but cannot directly require the relative velocity; to calculate the relative velocity, a FTC observer is introduced in the second step; next, the relative position and velocity information is sent to the CPU and the adaptive guidance law is carried out to generate the acceleration command; finally, the actuator receives the command and adjust the rendezvous dynamics. In the last step, actuator fault and time-varying target position are regard as disturbance and considered in simulations.

TABLE 1. Geostationary transfer orbital parameters.

Parameter	Value
Target orbital parameters	The semi-major axis $a = 2.4616 \times 10^7 m$, the eccentricity $e = 0.73074$, and the gravity constant $\mu = 3.984 \times 10^{14} m^3/s^2$
Initial relative kinematics	Initial relative position: $\begin{bmatrix} 50m & 70m & 90m \end{bmatrix}^T$, initial velocity: $\begin{bmatrix} 0 & 0 & 0 \end{bmatrix}^T$. Initial true anomaly: $\theta(0) = 0$.

Assume that the target spacecraft is rotated beyond the geostationary transfer orbit, which is a temporary obit to deliver a satellite into geosynchronous orbit. Some parameters used in the simulations about this orbit is given as Table.1.

The design parameters are given as Table.2.

TABLE 2. Design parameters.

Parameter	n	k	p	τ	l_0
Value	0.01	0.05	2.2	0.1	0.05

Parameter	r_0	γ	α_0	β_0	m
Value	0.05	0.08	2	1	0.99

Similar to [8], [16], considering that the external perturbations are always periodically varying [44], the unit of external disturbance can be assumed as following trigonometric form:

$$\mathbf{\Delta} = \begin{bmatrix} \Delta_x \\ \Delta_y \\ \Delta_z \end{bmatrix} = \begin{bmatrix} 0.005 \sin(0.2t) \\ 0.005 \sin(0.2t) \\ 0.005 [0.6 \sin(0.2t) + 0.6 \cos(0.2t)] \end{bmatrix} \quad (61)$$

To make the simulation more realistic, following measurement noise is considering in every simulation:

B. SIMULATION WITH COMPARISON
In order to show the superiority of the proposed rendezvous scheme, an output feedback rendezvous law based on an asymptotical convergence high-gain observer (please see [45] to find more details) is also performed in simulations as a contract. This rendezvous algorithm is formulated as

$$u_x = -\left(\omega^2 \hat{x} + 2\omega \dot{\hat{z}} + \dot{\omega} \hat{z} - \frac{\kappa \hat{x}}{R^3} \right) - \frac{h_3}{h_1^3} \hat{x} - \frac{h_4}{h_1} \dot{\hat{x}}$$

$$u_y = \frac{\kappa y}{R^3} - \frac{h_3}{h_1^3} \hat{y} - \frac{h_4}{h_1} \dot{\hat{y}}$$

$$u_x = -\left(\omega^2 \hat{z} + 2\omega \dot{\hat{x}} + \dot{\omega} \hat{x} - \frac{2\kappa \hat{z}}{R^3} \right) - \frac{h_3}{h_1^3} \hat{x} - \frac{h_4}{h_1} \dot{\hat{x}} \quad (62)$$

where, $\hat{x}$, $\hat{y}$ and $\hat{z}$ are estimated values of x, y and z, respectively; $\dot{\hat{x}}$, $\dot{\hat{y}}$ and $\dot{\hat{z}}$ are estimated values of $\dot{x}$, $\dot{y}$ and $\dot{z}$, respectively. Moreover, these estimated values are governed by a high-gain observer as shown as follows:

$$\dot{\hat{x}} = \dot{\hat{x}} + \frac{h_5}{h_2}(x - \hat{x})$$

$$\ddot{\hat{x}} = -\frac{h_3}{h_1^2} x - \frac{h_4}{h_1} \dot{\hat{x}} + \frac{h_6}{h_2^2}(x - \hat{x})$$

$$\dot{\hat{y}} = \dot{\hat{y}} + \frac{h_5}{h_2}(y - \hat{y})$$

$$\ddot{\hat{y}} = -\frac{h_3}{h_1^2} y - \frac{h_4}{h_1} \dot{\hat{y}} + \frac{h_6}{h_2^2}(y - \hat{y})$$

$$\dot{\hat{z}} = \dot{\hat{z}} + \frac{h_5}{h_2}(z - \hat{z})$$

$$\ddot{\hat{z}} = -\frac{h_3}{h_1^2} z - \frac{h_4}{h_1} \dot{\hat{z}} + \frac{h_6}{h_2^2}(z - \hat{z}) \quad (63)$$

Considering the control input of spacecraft is limited in real practice, the maximum of control input is set up as $u_{max} = 2m^2/s$. Furthermore, to attenuate the inherent chattering of sign function, the sigmoid function is introduced and take the place of sign function. The sigmoid function can be formulated as

$$sgmf(x) = 2\left(\frac{1}{1 + \exp(-x/\varepsilon)} - \frac{1}{2} \right) \quad (64)$$

where ε is a small positive constant.

The design parameters of ISSG and high-gain observer are selected as Table.3.

TABLE 3. Design parameters.

Parameter	κ	h_1	h_2	h_3	h_4	h_5	h_6
Value	0.1	1	1.5	0.005	0.1	2	1

The simulation results are shown as Figure. 3. The relative distance and relative velocity are presented in Fig.3(a) and (b), respectively. As shown in these figures, one can observe that both rendezvous laws can drive the relative distance and its rate converge to a small neighborhood around zero in finite time, however, it also can be observed from the zoom-in graphs that there exists chattering when the contracted ISS rendezvous law is used. From [16], it can be known that this chattering is resulted from the external disturbance. The proposed rendezvous law (18), however, can resist this bad influence effectively. Control inputs are illustrated in Fig.3 (c) as well as adaptive elements of three control channels in the proposed rendezvous law are depicted in Fig.3 (d). This figure clearly shows that the adaptive elements have lower bounds. Fig.3 (e) gives the response curves about estimation performance, one can conclude from these figures that both the proposed finite-time convergent

(a) Relative Position

(b) Relative Velocity

(c) Acceleration Input

(d) Adaptive element

(e) Velocity estimation
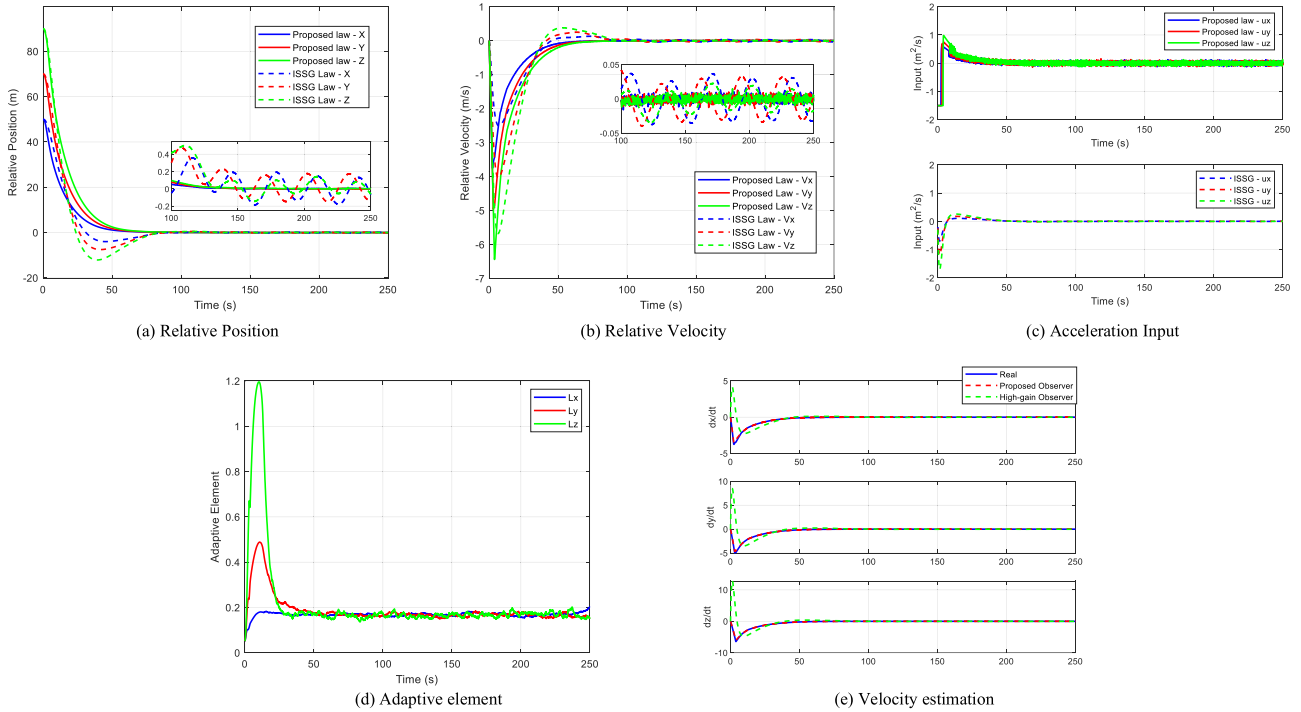
FIGURE 3. Simulation results without actuator faults.

observer (11) and the contracted high-gain observer (63) can accurately estimate the knowledge of relative kinematics, however, it can be seen that there exists an over-estimating scenario in high-gain observer (63).

C. SIMULATION WITH ACTUATOR FAULT CONSIDERATION
Because of time delay, sensor failure and other reasons, actuator failure may occur and result in undesirable performance during the rendezvous phase. According to the engineering experience, actuator fault usually shows up as four forms: saturation, nonlinearity, discontinuous and indeterminacy [38] and can be divided into two types: additive fault and out of control [8]. The former one refers that the bounded fault enter control channels in an additive way, while the latter one refers actuator loses its effectiveness. Taking actuator fault into account, total manipulated variable $\boldsymbol{u}$ which represents actuator effectiveness can be formulated as following form

$$\boldsymbol{u} = \boldsymbol{G}(t)\boldsymbol{u}_n + \boldsymbol{F}(t)\boldsymbol{u}_f \quad (65)$$

where $\boldsymbol{u}_n \in \mathbb{R}^3$ represents the nominal manipulated variable, $\boldsymbol{G}(t) \in \mathbb{R}^3$ represents the time profile of additive fault that occurs at some unknown time, $\boldsymbol{F}(t)\boldsymbol{u}_f \in \mathbb{R}^3$ represents the deviation in acceleration due to the presence of independent actuator fault. $\boldsymbol{u}_f \in \mathbb{R}^3$ represents the fault component. The matrix $\boldsymbol{F}(t) \in \mathbb{R}^3$ represents the time profile of independent fault that occurs at some unknown time. The fault-time profile $\boldsymbol{G}(t)$ and $\boldsymbol{F}(t)$ can be formulated as diagonal matrices of the

forms, respectively.

$$\boldsymbol{G}(t) = diag\left(g_x(t_x), g_y(t_y), g_z(t_z)\right)$$
$$\boldsymbol{F}(t) = diag\left(f_x(t_x), f_y(t_y), f_z(t_z)\right) \quad (66)$$

where $g_i : \mathbb{R} \to \mathbb{R}$ $(i = x, y, z)$ and $f_i : \mathbb{R} \to \mathbb{R}(i = x, y, z)$ are functions to describe the characteristic of total actuator fault.

For the time profile of actuator faults (65) with $\|\boldsymbol{F}\| \leq F_{\max}$ and $0 < g_i < 1$, assume that

$$\begin{aligned} f_i &= 0 & 0 \leq t \leq t_{fi}^0 \\ f_i &= 0.01 + 0.05\sin(0.2t) & otherwise \end{aligned} \quad (67)$$

with $t_{fx}^0 = 0s$, $t_{fy}^0 = 50s$, $t_{fz}^0 = 100s$ and

$$\begin{aligned} g_i &= 1 & 0 \leq t \leq T_{fi}^{01} \\ g_i &= 0.4 & T^{01}fi \leq t \leq T_{fi}^{02} \\ g_i &= 0.8 + 0.1\sin(0.2t) & otherwise \end{aligned} \quad (68)$$

with $T_{fx}^{01}, T_{fy}^{01}, T_{fz}^{01} = 20s$ and $T_{fx}^{02}, T_{fy}^{02}, T_{fz}^{02} = 70s$.

The comparison results in the presence of actuator faults are shown as Fig.4, similar to former case, the relative distance and relative velocity are presented in Fig.4 (a) and (b), respectively, control inputs are illustrated in Fig.4 (c) as well as adaptive elements of three control channels in the proposed rendezvous law are depicted in Fig.4 (d), the response curves about estimation performance are illustrated as Fig.4 (e). From these simulation results, particular from Fig.4 (a) and (b), one can clearly see that the contract

(a) Relative Position

(b) Relative Velocity

(c) Acceleration Input

(d) Adaptive element

(e) Velocity estimation
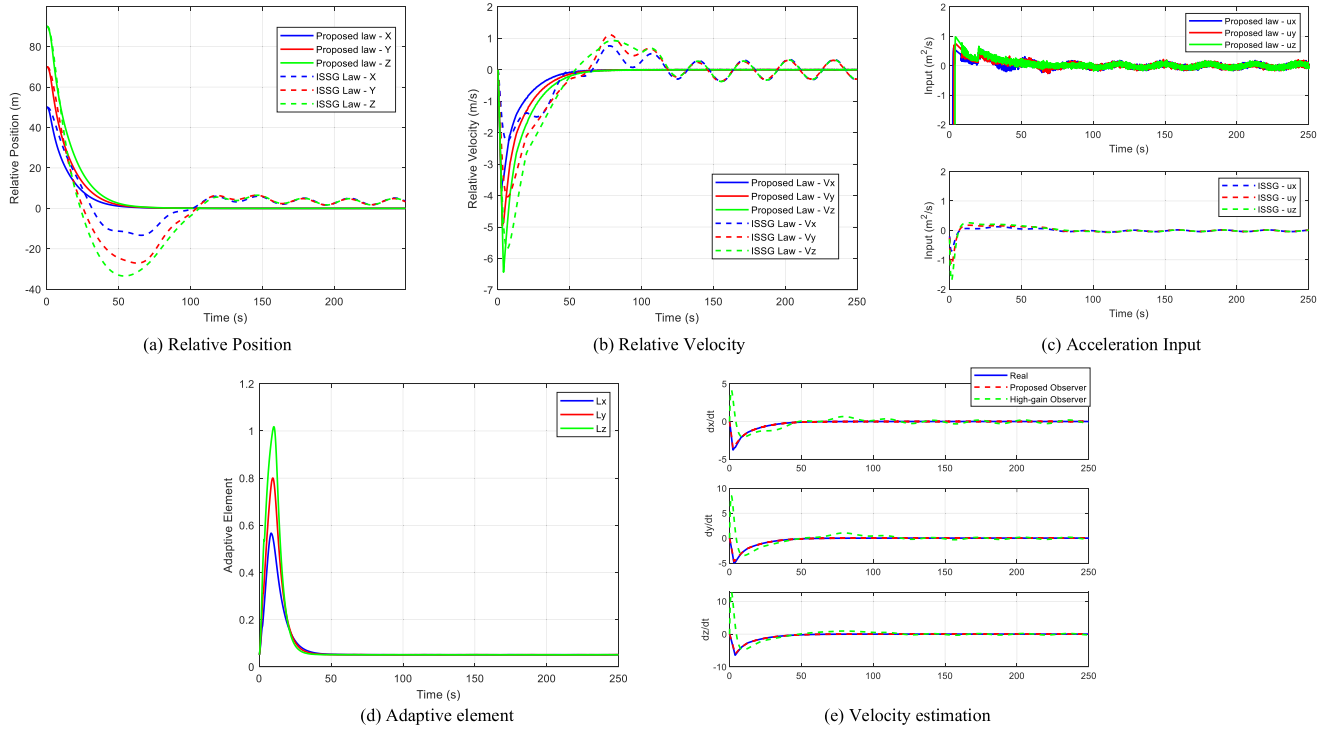
FIGURE 4. Simulation results with actuator faults.

(a) Relative Position

(b) Relative Velocity

(c) Acceleration Input

(d) Adaptive element

(e) Velocity estimation
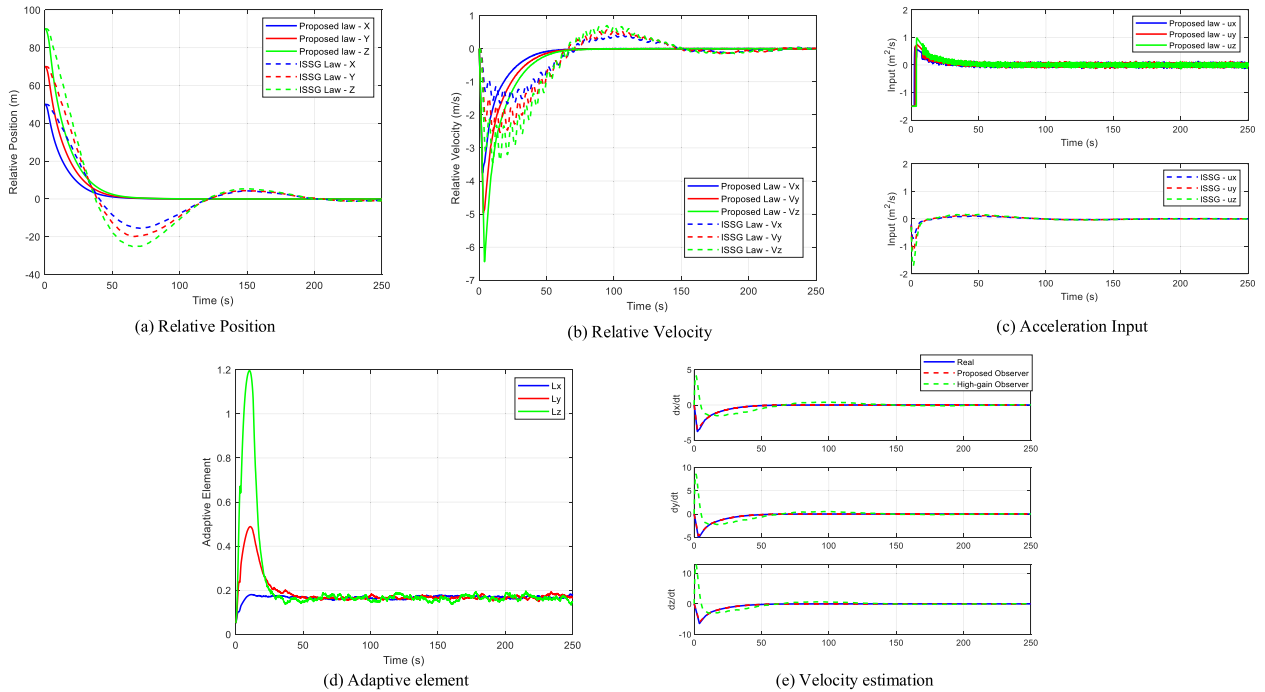
FIGURE 5. Simulation results considering second-order actuator dynamics.

rendezvous scheme loses its effectiveness and cannot force the relative distance and its rate converge into zero, whereas the proposed rendezvous guidance scheme shows its powerful fault-tolerant property and works as usual.

D. SIMULATION CONSIDERING SECOND-ORDER ACTUATOR DYNAMICS

For a practical control issue, we consider the high-order dynamics in simulation. Generally, second-order

(a) Scatter diagram of relative position

(b) Cumulative distribution of relative position

(c) Scatter diagram of relative velocity

(d) Cumulative distribution of relative velocity
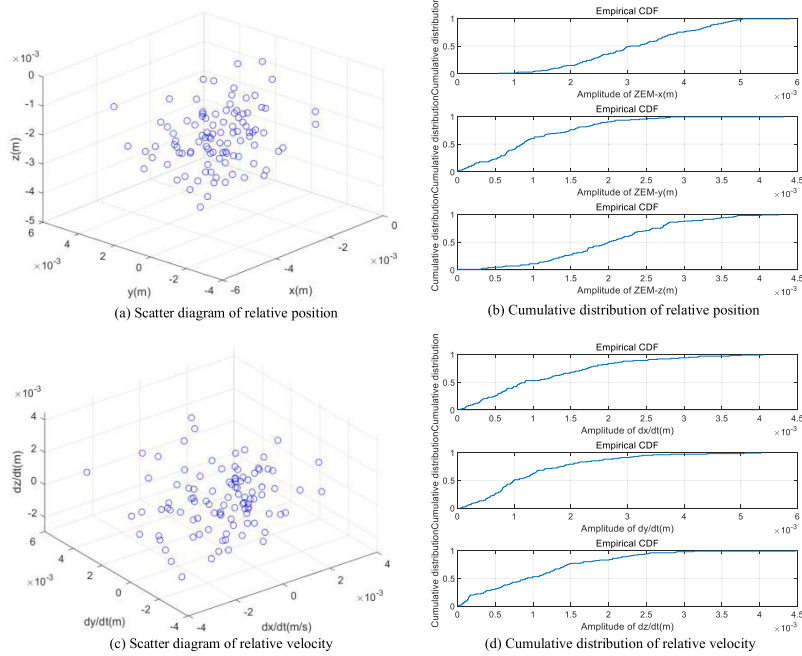
FIGURE 6. Monte-Carlo simulation results without actuator fault.

(a) Scatter diagram of relative position

(b) Cumulative distribution of relative position

(c) Scatter diagram of relative velocity

(d) Cumulative distribution of relative velocity
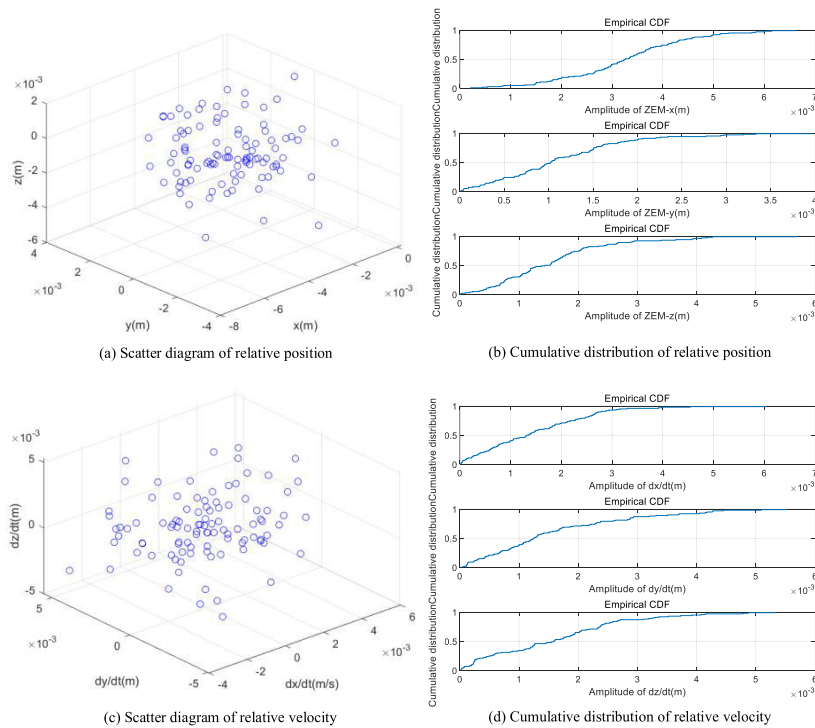
FIGURE 7. Monte-Carlo simulation results with actuator fault.

dynamics can describe the characteristics of actuator, although the characteristics of actuator are always much complex.

The second-order dynamics of the manipulated input $\boldsymbol{u}$ is formulated as following equations:

$$\ddot{\boldsymbol{u}} = -2\boldsymbol{\xi}_u \circ \boldsymbol{\omega}_u \circ \boldsymbol{u} - \boldsymbol{\omega}_u \circ \boldsymbol{u} + \boldsymbol{\omega}_u^2 \circ \boldsymbol{u}_c \qquad (69)$$

(a) Scatter diagram of relative position

(b) Cumulative distribution of relative position

(c) Scatter diagram of relative velocity

(d) Cumulative distribution of relative velocity
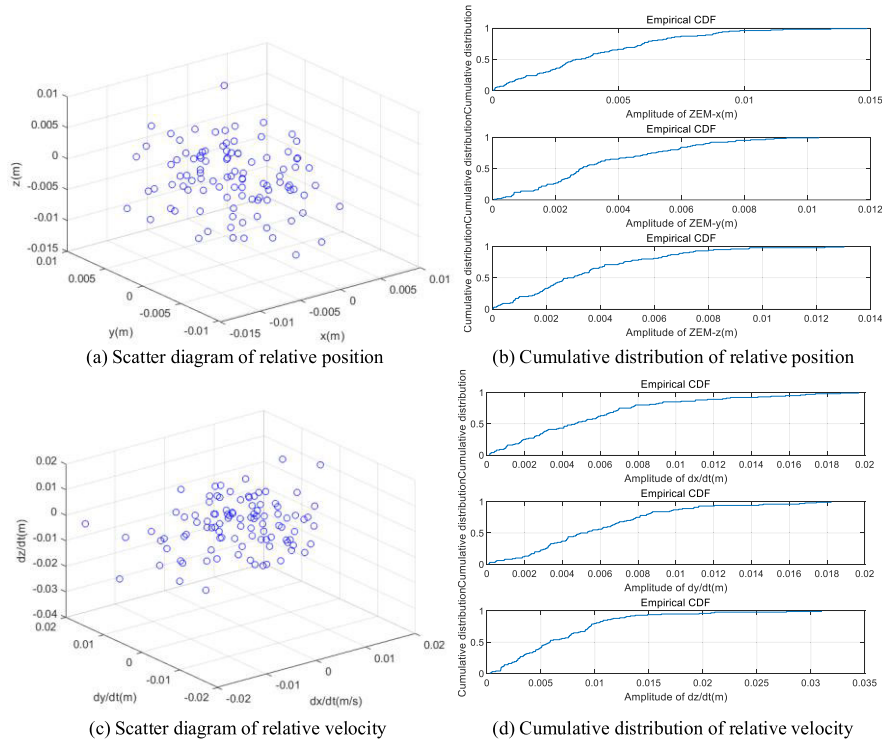
FIGURE 8. Monte-Carlo simulation results considering second-order actuator dynamics.

where $\boldsymbol{\xi}_u = col(\xi_{ux}, \xi_{uy}, \xi_{uz})$ being damping ratio, $\boldsymbol{\omega}_u = col(\omega_{ux}, \omega_{uy}, \omega_{uz})$ being natural frequency and $\boldsymbol{u}_c = col(u_{cx}, u_{cy}, u_{cz})$ being manipulated input command. For above system dynamics, following backstepping controller is presented to counteract the oscillation phenomenon of the second-order dynamics [46].

$$\boldsymbol{u}_c = \boldsymbol{\omega}_u^{-2} \begin{pmatrix} 2\boldsymbol{\xi}_u \circ \boldsymbol{\omega}_u \circ \dot{\boldsymbol{u}} + \boldsymbol{\omega}_u^2 \circ \dot{\boldsymbol{u}} + (\boldsymbol{u} - \boldsymbol{u}^*) \\ -\hbar_1 (\dot{\boldsymbol{u}} - \dot{\boldsymbol{u}}^*) - \hbar_2 |\dot{\boldsymbol{u}} - \dot{\boldsymbol{u}}^*|^{\hbar_3} sign (\dot{\boldsymbol{u}} - \dot{\boldsymbol{u}}^*) \end{pmatrix}$$
(70)

where $\boldsymbol{u}^*$ is the virtual rendezvous law and its formulation is same as (16). Similarly, the $\boldsymbol{u}^*$ in ISSG is same as (62). In this simulation example, $\hbar_1 = 5$, $\hbar_2 = 5$, $\hbar_3 = 2.1$, $\boldsymbol{\xi}_u = col(0.75, 0.75, 0.75)$ and $\boldsymbol{\omega}_u = col(0.8, 0.8, 0.8)$.

Similar to above two cases, the curves including relative position, relative velocity, acceleration input, adaptive element and relative velocity estimation are illustrated in Figures. 5(a)∼(e). Shown as Figures (a) and (b), the relative position and velocity of ISSG have a large-scale oscillation which is caused by actuator dynamics. As a comparison, the proposed guidance law can work as usual.

E. MOTE CARLO SIMULATION RESULTS

In real practice, uncertainty caused by measurement instrumental error and environment noise always exists and may result in missile performance degradation. Facing this scenario, guidance law should hold the strong property of robustness to tolerant un-certainty. To demonstrate the robustness of

TABLE 4. Lower and upper bounds of initial parameters.

Parameter	Lower bound	Upper bound	Parameter	Lower bound	Upper bound
x	45 m	55 m	$\dot{x}$	-2 m/s	2 m/s
y	63 m	77 m	$\dot{y}$	-2 m/s	2 m/s
z	81 m	99 m	$\dot{z}$	-2 m/s	2 m/s

the proposed "observer-controller" rendezvous system with actuator performance consideration, a Monte Carlo simulation example with 100 runs is performed.

The simulation condition is set up as follows: the inertial relative position and velocity subject to uniform distribution U∼[0, 1] is randomly chosen, whose lower and upper bounds are listed as Table 4; other parameters are selected as subsection B. The actuator fault and second-order dynamics are formulated as same in subsection C and D.

The Monte Carlo simulation result without actuator fault is shown as Fig.6. Figs.6(a) and (c) depict the scatter diagrams of the relative position and relative velocity at 250s, respectively. Relatively, Figs.6(b) and 6(c) depict the cumulative distributions of relative position and relative velocity at 250s, respectively. It is easy to find that the terminal relative position are distributed within 0.005m, and the terminal relative velocity are distributed within 0.006m/s.

The Monte Carlo simulation result considering actuator fault and dynamics are shown as Fig.7 and 8. Similar as Fig.6, it is easy to find that the terminal relative position are distributed within 0.006m, and the terminal relative velocity are distributed within 0.02m/s. This further demonstrates the robustness and effectiveness of the proposed "observer-controller" rendezvous system.

V. CONCLUSION

This paper proposed two types of continuous PIGC systems, whose inner loops are same but outer loop are different. Using integrated barrier Lyapunov function and backstepping design, a finite time convergent control algorithm for related second-order system is presented and is applied to PIGC system. In order to acquire the target maneuvers, a second-order sliding mode observer is proposed to force the estimated value approach to the real value. Numerical simulation results demonstrate the effectiveness of the proposed PIGC systems.

APPENDIX

Taking the derivatives of $\tilde{r}$ and $\tilde{v}$ with respect to time yielding

$$
\begin{aligned}
\dot{\tilde{r}} &= \dot{r} - \dot{\hat{r}} = \tilde{v} - a_1|\tilde{r}|^{1/2}sign(\tilde{r}) - a_2|\tilde{r}|^{3/2}sign(\tilde{r}) \\
\dot{\tilde{v}} &= \dot{v} - \dot{\hat{v}} = d - a_3 sign(\tilde{r})
\end{aligned} \tag{A.1}
$$

For the convenience of demonstration, define an auxiliary vector as

$$
e\begin{bmatrix} e_1 \\ e_2 \end{bmatrix} = \begin{bmatrix} |\tilde{r}|^{1/2}sign(\tilde{r}) \\ \tilde{v} \end{bmatrix} \tag{A.2}
$$

Taking the time derivative of (A.2) yielding

$$
\begin{aligned}
\dot{e} &= \begin{bmatrix} \dot{e}_1 \\ \dot{e}_2 \end{bmatrix} = \begin{bmatrix} \dfrac{1}{2|e_1|}(e_1 - a_1 e_1 - a_2 e_1^3) \\ d - \dfrac{a_3 e_1}{|e_1|} \end{bmatrix} \\
&= \frac{1}{|e_1|}(A_1 e + B_1) \tag{A.3}
\end{aligned}
$$

with two matrices

$$
A_1 = \begin{bmatrix} -\dfrac{a_1}{2} & \dfrac{1}{2} \\ -a_3 & 0 \end{bmatrix}, \quad B_1 = \begin{bmatrix} -\dfrac{a_2}{2}e_1^3 \\ d|e_1| \end{bmatrix} \tag{A.4}
$$

Since a_1, a_2 and a_3 are positive constants, it is easy to verify that the matrix A_1 is negative-definite (Hurwitz). Note that there exists an upper bound d_{max} of the external disturbance according to Assumption 1. Moreover, from Proposition 1, we know that there exists a certain but unknown constant e_{max} such that $\|e\| \leq e_{max}$. With these facts in mind, one can imply that there exist a positive constant τ such that $\|B_1\| \leq \max\left\{\tau\|e\|, \tau\|e\|^3\right\}$.

By defining P_1 as an arbitrary symmetric positive-definite matrix, a Lyapunov function candidate for system (A.1) is selected as following equation.

$$
V_1 = e^T P_1 e \tag{A.5}
$$

Taking the derivative of (A.5) with respect to time gives

$$
\begin{aligned}
\dot{V}_1 &= \frac{1}{|e_1|}(e^T(A^T P_1 + P_1 A)e + 2e^T P_1 B) \\
&= \frac{1}{|e_1|}(-e^T Q e + 2e^T P_1 B) \tag{A.6}
\end{aligned}
$$

where $Q = -(A^T P_1 + P_1 A)$ is also a symmetric positive-definite matrix. Hence, one can conclude that

$$
\dot{V}_1 \leq \frac{1}{|e_1|}\left(\lambda_{min}(Q)\|e\|^2 - 2\|e\|\|P_1\|\|B\|\right) \tag{A.7}
$$

Next, consider following two cases:

Case 1: If $0 \leq \|e\| \leq 1$, then $\|e\| \geq \|e\|^2$, hence, one can conclude that

$$
\dot{V}_1 \leq -\frac{1}{\|e\|}(\lambda_{min}(Q) - 2\tau\|P_1\|)\|e\|^2 \tag{A.8}
$$

Case 2: If $\|e\| > 1$, then $\|e\| < \|e\|^2$, hence, one can conclude that

$$
\dot{V}_1 \leq -\frac{1}{\|e\|}(\lambda_{min}(Q) - 2\tau\|P_1\|\|e\|^2)\|e\|^2 \tag{A.9}
$$

By defining a constant $\max\{\|e\|_{max}, 1\}$ and then selecting a suitable τ such that $\tau < \lambda_{min}(Q)/2K\|P_1\|^2$, it is ensured that $\dot{V}_1$ is negative-definite. Combining with (A.8) and (A.9), following inequality can be acquired

$$
\dot{V}_1 \leqslant -\frac{\Omega}{\|e\|}\|e\|^2 = \Omega\|e\| \leqslant -\frac{\Omega}{\lambda_{max}(P_1)}V_1^{\frac{1}{2}} \tag{A.10}
$$

with $\Omega = \min\left\{\lambda_{min}(Q) - 2\tau\|P_1\|, \lambda_{min}(Q) - 2\tau\|P_1\|\|e\|^2\right\}$. According to Lemma 1, the proposed observer can drive estimation error converge to a small compact neighborhood around zero.

Furthermore, according to Lemma 1, T_f can be formulated as

$$
T_f \leq 2\lambda_{max}(P_1)V_1^{1/2}(0)/\Omega \tag{A.11}
$$

where $V_1(0)$ represents the initial value of $V_1(t)$.

This completes the Proof.

ACKNOWLEDGMENT

REFERENCES

[1] L. Sun and Z. Zheng, "Adaptive sliding mode control of cooperative spacecraft rendezvous with coupled uncertain dynamics," *J. Spacecraft Rockets.*, vol. 54, no. 3, pp. 652–661, May 2017.

[2] D. Zhang, J. Luo, D. Gao, W. Ma, and J. Yuan, "A novel nonlinear control for tracking and rendezvous with a rotating non-cooperative target with translational maneuver," *Acta Astronautica*, vol. 138, pp. 276–289, Sep. 2017.

[3] K. Xia and W. Huo, "Robust adaptive backstepping neural networks control for spacecraft rendezvous and docking with input saturation," *ISA Trans.*, vol. 62, pp. 249–257, May 2016.

[4] L. Sun, W. Huo, and Z. Jiao, "Adaptive nonlinear robust relative pose control of spacecraft autonomous rendezvous and proximity operations," *ISA Trans.*, vol. 67, pp. 47–55, Mar. 2017.

[5] Z. Ya-kun, L. Hai-yang, H. Rui-xue, and L. Jiang-hui, "Shared control on lunar spacecraft teleoperation rendezvous operations with large time delay," *Acta Astronautica*, vol. 137, pp. 312–319, Aug. 2017.

[6] M. Li and H. Peng, "Solutions of nonlinear constrained optimal control problems using quasilinearization and variational pseudospectral methods," *ISA Trans.*, vol. 62, pp. 177–192, May 2016.

[7] S. He and D. Lin, "Reliable spacecraft rendezvous without velocity measurement," *Acta Astronautica*, vol. 144, pp. 52–60, Mar. 2018.

[8] W. H. Clohessy and R. S. Wiltshire, "Terminal guidance system for satellite rendezvous," *J. Aerosp. Sci.*, vol. 27, no. 9, pp. 653–658, Sep. 1960.

[9] T. E. Carter, "State transition matrices for terminal rendezvous studies: Brief survey and new example," *J. Guid., Control, Dyn.*, vol. 21, no. 1, pp. 148–155, Jan. 1998.

[10] D. J. Jezewski and J. D. Donaldson, "An analytical approach to optimal rendezvous using Clohessy-Wiltshimne equations," *J. Astron. Sci.*, vol. 27, no. 3, pp. 293–310, 1979.

[11] W. A. Scheel and B. A. Conway, "Optimization of very-low-thrust, many-revolution spacecraft trajectories," *J. Guid., Control, Dyn.*, vol. 17, no. 6, pp. 1185–1192, Nov. 1994.

[12] H. Gao, X. Yang, and P. Shi, "Multi-objective robust H_∞ control of spacecraft rendezvous," *IEEE Trans. Control Syst. Technol.*, vol. 17, no. 4, pp. 794–802, Jul. 2009.

[13] X. Gao, K. L. Teo, and G.-R. Duan, "Non-fragile robust H∞ control for uncertain spacecraft rendezvous system with pole and input constraints," *Int. J. Control*, vol. 85, no. 7, pp. 933–941, Jul. 2012.

[14] S. Ulrich, D. L. Hayhurst, A. Saenz Otero, D. Miller, and I. Barkana, "Simple adaptive control for spacecraft proximity operations," in *Proc. AIAA Guid., Navigat., Control Conf.*, Jan. 2014, p. 1288.

[15] L. Sun and W. Huo, "Adaptive fuzzy control of spacecraft proximity operations using hierarchical fuzzy systems," *IEEE/ASME Trans. Mechatronics*, vol. 21, no. 3, pp. 1629–1640, Jun. 2016.

[16] Y. Wang and H. Ji, "Integrated relative position and attitude control for spacecraft rendezvous with ISS and finite-time convergence," *Aerosp. Sci Technol.*, vol. 85, pp. 234–245, Feb. 2019.

[17] L. Sun, W. Huo, and Z. Jiao, "Robust adaptive relative position and attitude control for spacecraft autonomous proximity," *ISA Trans.*, vol. 63, pp. 11–19, Jul. 2016.

[18] H. Ma and S. Xu, "Optimization of bounded low-thrust rendezvous with terminal constraints by interval analysis," *Aerosp. Sci. Technol.*, vol. 79, pp. 58–69, Aug. 2018.

[19] G. Zhang and D. Ye, "Optimal short-range rendezvous using on-off constant thrust," *Aerosp. Sci. Technol.*, vol. 69, pp. 208–217, Oct. 2017.

[20] R. Epenoy, "Fuel optimization for continuous-thrust orbital rendezvous with collision avoidance constraint," *J. Guid., Control, Dyn.*, vol. 34, no. 2, pp. 493–503, Mar. 2011.

[21] B. Xiao and S. Yin, "Velocity-free fault-tolerant and uncertainty attenuation control for a class of nonlinear systems," *IEEE Trans. Ind. Electron.*, vol. 63, no. 7, pp. 4400–4411, Jul. 2016.

[22] S. Jacobsen, C. Lee, C. Zhu, and S. Dubowsky, "Planning of safe kinematic trajectories for free flying robots approaching an uncontrolled spinning satellite," in *Proc. ASME Int. Design Eng. Tech. Conf. Comput. Inf. Eng. Conf. Amer. Soc. Mech. Eng.*, 2002, Art. no. 34336.

[23] L. Cao, D. Qiao, and J. Xu, "Suboptimal artificial potential function sliding mode control for spacecraft rendezvous with obstacle avoidance," *Acta Astronautica*, vol. 143, pp. 133–146, Feb. 2018.

[24] L. Sun, W. Huo, and Z. Jiao, "Adaptive backstepping control of spacecraft rendezvous and proximity operations with input saturation and full-state constraint," *IEEE Trans. Ind. Electron.*, vol. 64, no. 1, pp. 480–492, Jan. 2017.

[25] M. Xin and H. Pan, "Nonlinear optimal control of spacecraft approaching a tumbling target," *Aerosp. Sci. Technol.*, vol. 15, no. 2, pp. 79–89, Mar. 2011.

[26] M. Xin and H. Pan, "Indirect robust control of spacecraft via optimal control solution," *IEEE Trans. Aerosp. Electron. Syst.*, vol. 48, no. 2, pp. 1798–1809, Apr. 2012.

[27] M. Xin and S. Balakrishnan, "A new method for suboptimal control of a class of nonlinear system," *Optim. Control Appl. Methods*, vol. 26, pp. 55–83, Mar. 2005.

[28] L. Zhao, Y. Jia, and F. Matsuno, "Adaptive time-varying sliding mode control for autonomous spacecraft rendezvous," in *Proc. 52nd IEEE Conf. Decis. Control*, Dec. 2013, pp. 5504–5509.

[29] S. He, D. Lin, and J. Wang, "Autonomous spacecraft rendezvous with finite time convergence," *J. Franklin Inst.*, vol. 352, no. 11, pp. 4962–4979, Nov. 2015.

[30] A. Imani and M. Bahrami, "Optimal sliding mode control for spacecraft formation flying in eccentric orbits," *Proc. Inst. Mech. Eng., I, J. Syst. Control Eng.*, vol. 227, no. 5, pp. 474–481, May 2013.

[31] C. Edwards and Y. Shtessel, "Adaptive continuous higher order sliding mode control," *Automatica*, vol. 65, pp. 182–190, Mar. 2016.

[32] V. I. Utkin and A. S. Poznyak, "Adaptive sliding mode control with application to super-twist algorithm: Equivalent control method," *Automatica*, vol. 49, no. 1, pp. 39–47, Jan. 2013.

[33] Y. Shtessel, M. Taleb, and F. Plestan, "A novel adaptive-gain supertwisting sliding mode controller: Methodology and application," *Automatica*, vol. 48, no. 5, pp. 759–769, May 2012.

[34] C. Edwards and Y. Shtessel, "Adaptive dual layer second-order sliding mode control and observation," in *Proc. Amer. Control Conf. (ACC)*, Jul. 2015, pp. 5853–5858.

[35] C. Edwards and Y. Shtessel, "Adaptive dual-layer super-twisting control and observation," *Int. J. Control*, vol. 89, no. 9, pp. 1759–1766, Sep. 2016.

[36] S. P. Bhat and D. S. Bernstein, "Finite-time stability of continuous autonomous systems," *SIAM J. Control Optim.*, vol. 38, no. 3, pp. 751–766, Jan. 2000.

[37] S. Yu, X. Yu, B. Shirinzadeh, and Z. Man, "Continuous finite-time control for robotic manipulators with terminal sliding mode," *Automatica*, vol. 41, no. 11, pp. 1957–1964, Nov. 2005.

[38] C. Qian and W. Lin, "A continuous feedback approach to global strong stabilization of nonlinear systems," *IEEE Trans. Autom. Control*, vol. 46, no. 7, pp. 1061–1079, Jul. 2001.

[39] W. Wang, Y. Ji, D. Lin, Z. Shi, and S. Lin, "A novel approximate finite-time convergent guidance law with actuator fault," *Cluster Comput.*, vol. 22, no. S4, pp. 10095–10107, Jul. 2019, doi: 10.1007/s10586-017-1114-y.

[40] A. Levant, "Sliding order and sliding accuracy in sliding mode control," *Int. J. Control*, vol. 58, no. 6, pp. 1247–1263, Dec. 1993.

[41] J. A. Moreno and M. Osorio, "Strict Lyapunov functions for the super-twisting algorithm," *IEEE Trans. Autom. Control*, vol. 57, no. 4, pp. 1035–1040, Apr. 2012.

[42] T. Gonzalez, J. A. Moreno, and L. Fridman, "Variable gain super-twisting sliding mode control," *IEEE Trans. Autom. Control*, vol. 57, no. 8, pp. 2100–2105, Aug. 2012.

[43] S. He, D. Lin, and J. Wang, "Continuous second-order sliding mode based impact angle guidance law," *Aerosp. Sci. Technol.*, vol. 41, pp. 199–208, Feb. 2015.

[44] S. Li and Y.-P. Tian, "Finite-time stability of cascaded time-varying systems," *Int. J. Control*, vol. 80, no. 4, pp. 646–657, Apr. 2007.

[45] S. He, J. Wang, and D. Lin, "Elliptical orbital spacecraft rendezvous without velocity measurement," *J. Aero. Eng.*, vol. 29, no. 4, 2015, Art. no. 04015084.

[46] Y. Ji, D. Lin, W. Wang, S. Hu, and P. Pei, "Three-dimensional terminal angle constrained robust guidance law with autopilot lag consideration," *Aerosp. Sci. Technol.*, vol. 86, pp. 160–176, Mar. 2019.

WEI WANG was born in Yulin, Shaanxi, China, in 1984. He received the M.S. and Ph.D. degrees in aerospace engineering from the School of Aerospace Engineering, Beijing Institute of Technology, Beijing, in 2009 and 2015, respectively. He is currently a Lecturer with the School of Aerospace Engineering, Beijing Institute of Technology. His research interests include flight vehicle design, aerodynamics, guidance and control, and electrical design.

YI JI was born in Changchun, Jilin, China, in 1994. He received the B.S. and M.S. degrees in aerospace engineering from the School of Aerospace Engineering, Beijing Institute of Technology, Beijing, in 2015 and 2017, respectively. He is currently pursuing the Ph.D. degree with the School of Aerospace Engineering, Beijing Institute of Technology. His research interests include flight vehicle guidance and control and advanced control theory.

DEFU LIN was born in Songyuan, Jilin, China, in 1971. He received the Ph.D. degree in flying vehicle design from the School of Aerospace Engineering, Beijing Institute of Technology, Beijing, in 2005. He is currently a Professor with the School of Aerospace Engineering, Beijing Institute of Technology, and the Director of the Beijing Key Laboratory of UAV Autonomous Control, Ministry of Education, Beijing. His research interests include overall design of flying vehicle, flight vehicle guidance and control, aerodynamics, and autonomous UAV control technique.

XINGWEI SHI was born in Xi'an, Shaanxi, China, in 1994. He received the B.S. degree in aerospace engineering from the School of Aerospace Engineering, Beijing Institute of Technology, Beijing, in 2017. He is currently a Graduate Student with the School of Aerospace Engineering, Beijing Institute of Technology. His research interests include nonlinear control and its application in aircraft guidance and control.

JIANTING ZHAO was born in Yingkou, Liaoning, China, in 1994. He received the B.S. degree in aerospace engineering from the School of Aerospace Engineering, Shenyang Aerospace University, Shenyang, in 2017. He is currently a Graduate Student with the School of Aerospace Engineering, Beijing Institute of Technology, Beijing. His research interests include nonlinear control and its application in aircraft guidance and control.

● ● ●